Electronic and optical switching of solution-phase deposited $SnSe_2$ phase change memory material

Robert Y. Wang,[1] Marissa A. Caldwell,[2] Rakesh Gnana David Jeyasingh,[3] Shaul Aloni,[1] Robert M. Shelby,[4] H.-S. Philip Wong,[3] and Delia J. Milliron[1,a)]

[1]*The Molecular Foundry, Lawrence Berkeley National Laboratory, Berkeley, California 94720, USA*
[2]*Department of Chemistry, Stanford University, Stanford, California 94305, USA*
[3]*Department of Electrical Engineering, Stanford University, Stanford, California 94305, USA*
[4]*IBM Almaden Research Center, San Jose, California 95120, USA*

(Received 24 January 2011; accepted 6 April 2011; published online 1 June 2011)

We report the use of chalcogenidometallate clusters as a solution-processable precursor to $SnSe_2$ for phase change memory applications. This precursor is spin-coated onto substrates and then thermally decomposed into a crystalline $SnSe_2$ film. Laser testing of our $SnSe_2$ films indicate very fast recrystallization times of 20 ns. We also fabricate simple planar $SnSe_2$ electronic switching devices that demonstrate switching between ON and OFF resistance states with resistance ratios varying from 7−76. The simple cell design resulted in poor cycling endurance. To demonstrate the precursor's applicability to advanced via-geometry memory devices, we use the precursor to create void-free $SnSe_2$ structures inside nanowells of ∼25 nm in diameter and ∼40 nm in depth. © *2011 American Institute of Physics*. [doi:10.1063/1.3587187]

I. INTRODUCTION

Phase change materials used for data storage can repeatedly and quickly switch between their amorphous and crystalline states.[1,2] The most established phase change material application is optical storage media such as rewritable compact disks, digital versatile disks, and Blu-ray disks. Although optical data storage using phase change materials is a mature technology, electronic data storage using phase change random access memory (PCRAM) is an emerging one.[1] PCRAM data is stored using the contrast in electrical resistivity between the amorphous (i.e., "OFF") and crystalline (i.e., "ON") states.[3] Many phase change materials can be found in the Ge−Sb−Te ternary phase diagram, with the most common alloy being $Ge_2Sb_2Te_5$.[2] Recent works have suggested $SnSe_2$ for phase change memory, but only report very limited data on its switching properties.[4,5] We demonstrate a solution-deposition process for $SnSe_2$ and report its optical and electronic switching properties.

II. EXPERIMENT

We use a soluble chalcogenidometallate cluster salt as a precursor to $SnSe_2$.[6–10] To synthesize the precursor, bulk SnSe was reacted with Se in hydrazine (*Caution: hydrazine is highly toxic and should be handled with extreme care*). A 2 M Se solution was prepared by dissolving Se (Strem, 93-3417) in hydrazine (Sigma-Aldrich, 215 155). Then, 2.2 mL of this solution was added to 2.2 mmol of SnSe (Alfa Aesar, 18 781) in a nitrogen-filled glovebox. Prior to use, the hydrazine was purified by distillation and the SnSe was crushed into small particles. After stirring for ∼ 1 day, the resulting orange solution was filtered through a 200 nm PVDF filter to remove any undissolved solids. The solid precursor was then isolated by drying under flowing nitrogen gas.

A 100 mg/mL precursor solution was prepared by dissolving the precursor in a 5:3 volumetric mixture of dimethyl sulfoxide:ethanolamine. The resulting yellow solution was then filtered through a 200 nm PVDF filter and spin-coated onto the substrates. The films were dried at 100 °C for a few minutes and then thermally decomposed into polycrystalline $SnSe_2$ by heating to 300 °C for 25 min on a hot plate.

Materials characterization was done using a combination of thermogravimetric analysis (TGA), x-ray diffraction (XRD), atomic force microscopy (AFM), scanning electron microscopy (SEM), and energy dispersive x-ray spectroscopy (EDS). TGA was performed under flowing nitrogen gas using a TA instruments model Q5000. XRD patterns were collected with a Bruker D8-Advance x-ray diffactometer equipped with a GADDS area detector and operated at 40 kV and 20 mA at the Cu Kα wavelength, 1.54 Å. SEM images and EDS analysis were done using a Zeiss Ultra 55 scanning electron microscope, equipped with an EDAX Sapphire detecting unit. AFM images were taken in tapping mode using a Veeco Multimode scanning probe microscope.

The optical switching properties of the $SnSe_2$ films were determined by static laser testing. During these tests, a laser pulse of variable time and power was applied to the film while a low power continuous wave laser was used to monitor the film reflectivity. The wavelengths of the pulse and continuous wave lasers were 658 and 635 nm, respectively. The substrates for static laser testing were silicon substrates with a 30 nm layer of sputtered SiO_2. Prior to depositing 50 nm thick $SnSe_2$ films, the substrates were cleaned using a UV-ozone treatment.

Electronic switching devices were patterned using optical lithography on silicon substrates with a 120 nm thick layer of thermally grown oxide. The switching devices were recessed into the substrate by etching 60 nm deep into the

a)Author to whom correspondence should be addressed. Electronic mail: dmilliron@lbl.gov.

 © 2011 American Institute of Physics

oxide layer. Initial attempts to pattern the $SnSe_2$ film by conventional lift-off procedures were unsuccessful owing to the solubility of common photoresist materials in the dimethyl sulfoxide:ethanolamine solvent mixture used to deposit the precursor. Patterning was instead achieved by using patterned hexamethyldisilazane (HMDS). This patterning caused a contrast in the adhesion quality of $SnSe_2$ to the substrate, which enabled the removal of $SnSe_2$ from HMDS patterned areas by sonication in ethanolamine. Top electrodes (10 nm Ti/100 nm Au) were then patterned on top of the $SnSe_2$ film using optical lithography and conventional lift-off. Prior to electrical testing, a 5 nm capping layer of sputtered SiO_2 was applied on top of the devices.

To emulate the conformal-deposition requirement of advanced via-geometry PCRAM device architectures,[1,11] we deposited our $SnSe_2$ into cylindrical nanowells of ~25 nm in diameter and ~40 nm in depth. The nanowells were prepared inside silicon oxide films as described in our previous work.[12] In brief, a polystyrene etch mask was prepared using block copolymer self-assembly of polystyrene-b-polymethylmethacrylate (PS-b-PMMA, Polymer Source, MW = 46 100:21000 PS:PMMA) and then subsequently removing the polymethylmethacrylate. The nanowell array was then created by CHF_3 reactive ion etching through the remaining polystyrene mask. After reactive ion etching, a UV-ozone treatment was used to remove the polystyrene mask and clean the nanowell array. $SnSe_2$ was then deposited into the nanowell array by spin-coating and decomposing the precursor.

Cross-sectional transmission electron microscope (TEM) images and analysis were performed on a JEOL2100 F with a liquid nitrogen cooled Oxford Instruments INCA-EDS detector. Sample cross sections were prepared by Nanolab Technologies[13] using focused ion beam (FIB) processing. Prior to FIB preparation, a protective layer containing silicon, oxygen, and carbon was evaporated onto the sample surface. Compositional mapping images were taken with a ~0.7 nm resolution and used the *K* edges of silicon, oxygen and carbon, and the *L* edges of tin and selenium.

III. RESULTS AND DISCUSSION

A. Materials characterization

TGA shows the decomposition process of the precursor (Fig. 1). During this experiment, the precursor was crushed into small particles and then its mass was continuously monitored as the temperature was increased. A temperature ramp from room temperature at a rate of 2 °C/min was followed by a 120 min isotherm at 300 °C, and then heating was resumed up to 350 °C. The 300 °C temperature isotherm mimics the decomposition temperature used during $SnSe_2$ film deposition. Approximately 25 min into the 300 °C isotherm step, the precursor's mass reached its final value, which indicates that these conditions are sufficient to fully decompose the precursor. The precursor loses ~43% of its original mass during decomposition.

XRD of the precursor before and after decomposition (Fig. 2) illustrates its structural metamorphosis and EDS confirms the 1:2 elemental ratio of Sn:Se. $SnSe_2$ has a hexagonal unit cell and is a layered crystal with repeating Se−Sn−Se trilayers.[5] The intense (0 0 2) and (0 0 3) peaks in the XRD pattern indicate that our thin films preferentially oriented with the *c* axis perpendicular to the substrate. Although this work focuses on thin films of $SnSe_2$, we note that thick films (prepared by drop casting) exhibited no preferential orientation.

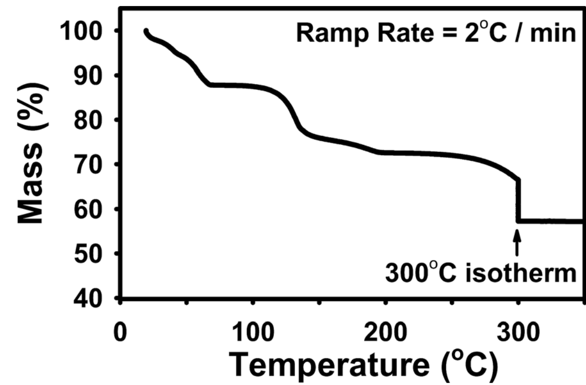

FIG. 1. Thermogravimetric analysis of the $SnSe_2$ precursor.

B. Optical switching

We investigated the amorphization and recrystallization speeds of our $SnSe_2$ films using static laser testing. Amorphization of an as-deposited crystalline $SnSe_2$ film is shown in Fig. 3(a). The laser pulses in this test cause both a local change in reflectivity and topography. The reflectivity changes were directly observed during laser testing, whereas topographical changes were observed afterwards by AFM (Fig. 4). Film amorphization of the as-deposited crystalline film could be observed by a local increase in film thickness at the laser pulse location [Fig. 4(a)]. The film thickness increase at these locations is consistent with the lower density of amorphous $SnSe_2$ compared to crystalline $SnSe_2$.[4] The mean heights of the amorphous bumps are 8.8 ± 2.1 nm.

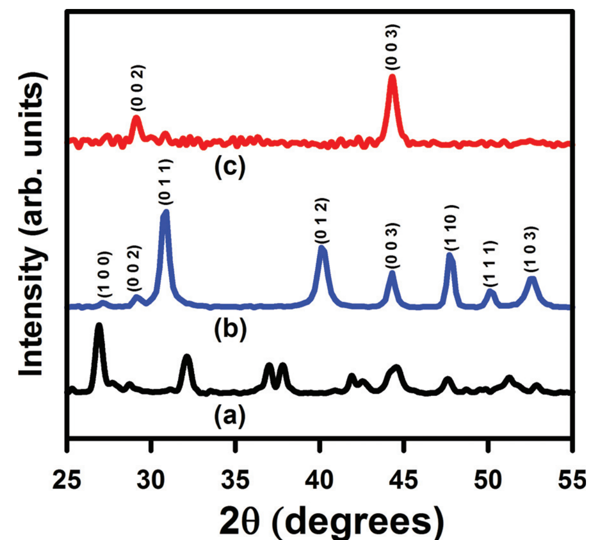

FIG. 2. (Color online) XRD of (a) the dried precursor, (b) a thick film of $SnSe_2$, and (c) a thin film of $SnSe_2$. Peaks were indexed using JCPDS file 01-089-3197.

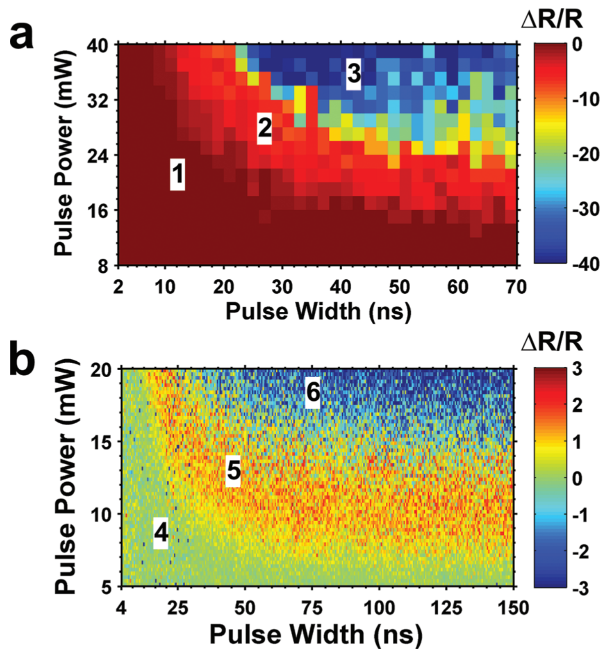

FIG. 3. (Color online) Laser pulse testing of the of $SnSe_2$ films. Each pixel represents a film location exposed to a particular pulse power and duration. The pixel color indicates the percent change in reflectivity ($\Delta R/R$) induced by that laser pulse. (a) Shows amorphization of a crystalline film, whereas (b) shows recrystallization following an amorphization pulse. The film was locally amorphized using a prepulse of 30 ns and 25 mW prior to each recrystallization pulse in (b).

Since the film was 50 nm thick, this corresponds to crystalline $SnSe_2$ being $15 \pm 3\%$ thinner than laser-amorphized $SnSe_2$, which is in agreement with data on $SnSe_2$ grown by molecular beam epitaxy.[4] Ablation of the crystallized film occurred at high pulse power and duration and could be observed by crater formation [Fig. 4(b)]. Three different regions of reflectivity change are observed in the laser pulse amorphization study. By correlating the AFM images with the reflectivity maps, we conclude that regions 1, 2, and 3 correspond to no change in the film, film amorphization, and film ablation, respectively. Amorphization is accompanied by a small decrease in reflectivity; the reflectivity of the as-deposited crystalline film and laser-amorphized film are 0.462 ± 0.011 and 0.434 ± 0.009, respectively.

Small reflectivity variations are observed throughout Fig. 3 and we attribute this to the film's microstructure, which has needlelike asperities (see Fig. 4). The needlelike structures ranged in size from 613 ± 282 nm $\times$ 145 ± 50 nm $\times$ 26 ± 7 nm (length $\times$ width $\times$ height). The AFM measurements reveal an overall root-mean-squared film roughness of $\sim$6 nm, which is not negligible when compared to the thickness of the film, which was 50 nm. No chemical composition differences between the needlelike structures and the film were observed by EDS.[14]

Laser recrystallization was used to evaluate the recrystallization speed of $SnSe_2$ [Fig. 3(b)]. To decrease the effect of the above-described reflectivity variations on the recrystallization time measurement, we measured numerous data points to make the different regions clearly identifiable in Fig. 3(b). Since the film was crystalline as-deposited, the film was locally amorphized with a laser prepulse (25 mW, 30 ns) prior to each recrystallization pulse. The amorphization effect for this laser pulse power and duration can be seen in Fig. 4(a). Three different regions, labeled 4 though 6, are observed in Fig. 3(b). A positive change in reflectivity, which indicates recrystallization, is observed in region 5. The reflectivity of the laser-recrystallized film is 0.443 ± 0.011, which is slightly lower than the as-deposited crystalline film. This difference in reflectivity could be due

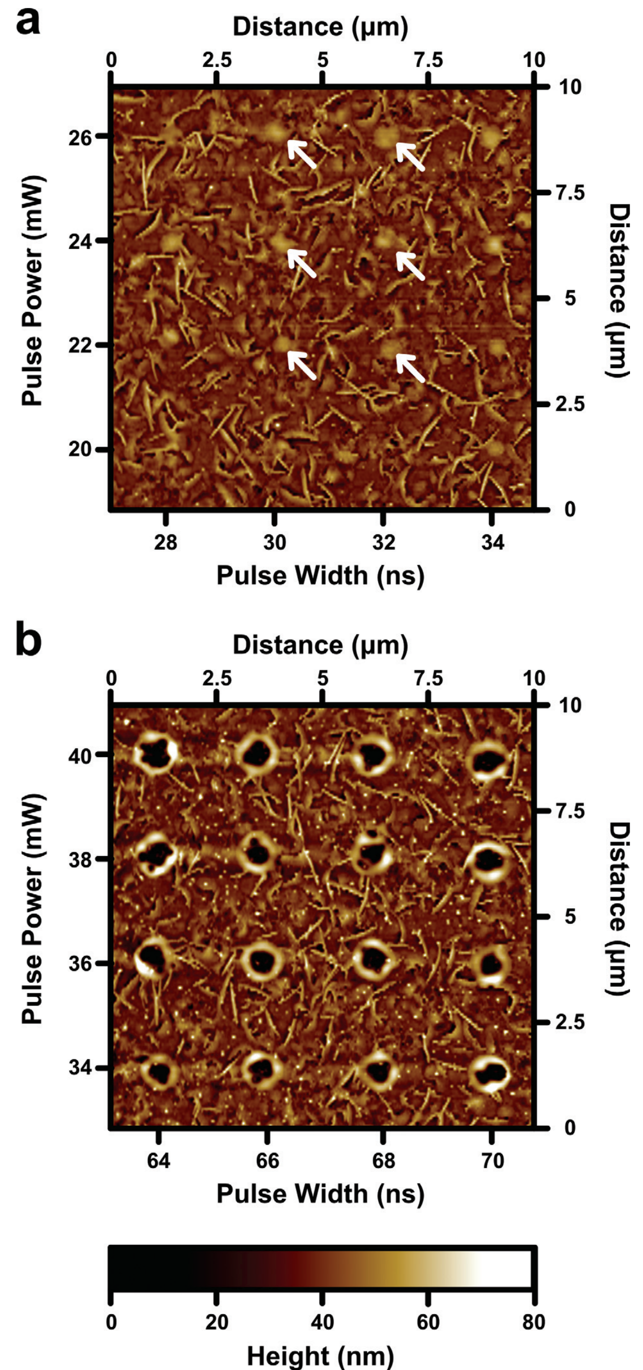

FIG. 4. (Color online) (a) AFM image of the amorphization region in Fig. 3(a). Several laser-induced amorphized spots, which are visible as elevated bumps, are labeled with arrows. (b) AFM image of the ablation region of Fig. 3(a). The large differences in laser pulse power and duration between parts (a) and (b) caused the ablated spot size to be larger than the amorphized spot size in these images (Ref. 14). The horizontal raised areas between ablated areas are image artifacts from the AFM scan direction.

to partial recrystallization and/or topographical differences between the as-deposited crystalline and laser-recrystallized films. AFM measurements of laser-recrystallized $SnSe_2$ reveal residual elevated areas at the laser spot locations.[14] Residual bumps after laser-recrystallization have also been observed in $Ge_2Sb_2Te_5$.[15] The reflectivity change, pulse power, and pulse duration of region 6 is very similar to that of region 2. Hence we associate region 6 with an increase in the volume of amorphized material.

Figure 3(b) demonstrates that $SnSe_2$ can recrystallize in as little as 20 ns. This is a significant improvement on prior studies of solution-phase deposited phase change materials, which suffered from slow recrystallization times.[6,10] Memory write-time is rate-limited by recrystallization, so fast times are necessary.[1,2] In fact, this 20 ns recrystallization time is comparable to that of $Ge_2Sb_2Te_5$, which is the prototypical phase change material.[1,2,16] Although $SnSe_2$ has a small optical contrast between the amorphous and crystalline states, its resistivity contrast is 10^5, which makes it of interest for PCRAM applications.[4]

C. Electronic switching

$SnSe_2$-based PCRAM has not been previously demonstrated — even for conventionally sputter deposited material. So, to explore this possibility, we fabricated rudimentary electronic-switching demonstration devices. These devices were made by optical lithography and are planar in geometry (Fig. 5). The bottleneck region of the device is the active area where electronically induced Joule heating causes the phase change. Devices were fabricated in which the bottleneck length and width were varied from 2–10 μm and 2–3 μm, respectively. The film thickness was between 20–60 nm.

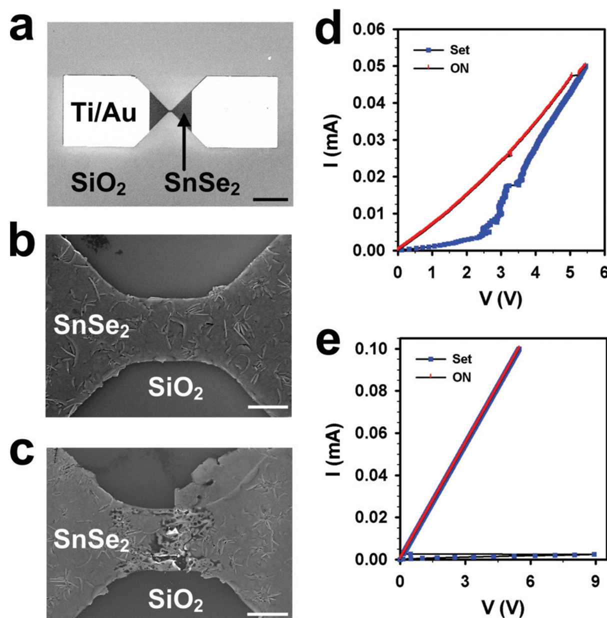

FIG. 5. (Color online) Top view scanning electron microscopy images of (a) a planar electronic switching cell, (b) active area of an electronic switching cell, and (c) active area of a failed electronic switching cell. Current–voltage characteristics of two different devices during the set process and in the ON state are shown in parts (d) and (e). The scale bar in (a), (b), and (c) are 50, 2, and 2 μm, respectively.

Since the as-deposited $SnSe_2$ is crystalline, the initial state of the devices was the ON state.

Devices were switched from ON to OFF (i.e., reset process) by applying a series of 50 ns voltage pulses ranging from 10–70 V. DC current sweeps were used to switch the devices from OFF to ON (i.e., set process). Figure 5 shows the set process of two example devices. Devices showed variable properties with resistance ratios ranging from 7–76. In many cases, a clear threshold switching snap-back is observed [Fig. 5(e)]. Although this resistance ratio is less than the 10^5 ratio observed in the sheet resistances of fully amorphous and fully crystalline $SnSe_2$,[4] it is sufficient to operate a memory device. A similar resistance ratio discrepancy is observed in $Ge_2Sb_2Te_5$, which is reported to be 10^5 in sheet resistance measurements,[17] but is generally only 10^1–10^2 when incorporated into a memory device.[18]

We note that the initial resistance of the switching devices prior to cycling was generally 10–30 kΩ. However after a single reset-set cycle, the resistance was generally 50–200 kΩ. This difference in resistance is likely due to two reasons. One reason is that during the set process only a crystalline percolation path is created through the amorphous active area (i.e., as opposed to crystallization of the entire active area). Another reason is that the active area experiences structural damage from the reset-set cycle (vide infra). We also prepared blanket films of as-deposited crystalline $SnSe_2$ to determine their electrical resistivity. Van der Pauw measurements on these films indicated a resistivity of 30 mΩ cm, which is in reasonable agreement with films prepared by molecular beam epitaxy and sputtering.[4]

All devices tested could reversibly switch between high and low resistance states. Unfortunately the elementary device design resulted in poor device endurance; devices generally failed after 1–2 switching cycles due to loss of $SnSe_2$ material [see Fig. 5(c)]. This failure mode may be attributed to large $SnSe_2$ absolute volume changes during switching (amorphous and crystalline $SnSe_2$ have a 17% density difference).[4] As described in literature on battery electrodes, large absolute changes in volume during cycling leads to material fracture and pulverization.[19] As the active area is scaled down to conventional PCRAM cell dimensions (characteristic length $<$100 nm),[11] we anticipate that both the reset power and sensitivity to absolute volume changes to improve. The reset power will decrease because the volume of material to be switched will decrease.[1] Literature on battery anodes shows that as the volume of a material is decreased, the material can better accommodate relative volumetric changes without fracturing.[19]

D. Via-filling

Many advanced PCRAM cell architectures utilize deep vias and/or trench geometries filled with phase change material.[1,11] This geometry is favorable because it reduces the cell's reset power, which ultimately leads to greater storage density.[1,11,20] One disadvantage of this cell architecture is that keyhole voids can form when filling these vias using conventional sputter deposition processes.[21] This obstacle can be overcome by using solution-phase deposition, during

which capillary forces drive the solution into the high aspect ratio holes and create void-free structures.[6,22] Although other techniques such as atomic layer deposition, chemical vapor deposition, and electrodeposition can accomplish this,[1,22] solution-phase deposition techniques benefit from their simplicity and inherently low cost.

To emulate the via-filling requirement of advanced PCRAM architectures, we used our $SnSe_2$ deposition process to fill cylindrical nanowells of ~25 nm in diameter and ~40 nm in depth. The conformal qualities of our solution-deposition process are demonstrated by Fig. 6(a), which shows the void-free deposition of $SnSe_2$ into the nanowells. The complementary shapes of the Sn, Se, Si, and O elemental composition maps further validates the high-quality $SnSe_2$ deposition [see Fig. 6(b)]. Some $SnSe_2$-filled nanowells exhibited defects [see Fig. 6(c)], but we anticipate that optimizing the deposition conditions could further improve on this result. Also apparent from this analysis are (1) a thin native oxide layer that formed between the oxide etch and $SnSe_2$ deposition steps and (2) the protective capping layer (visible in the Si, O, and C elemental maps) used during FIB cross-section preparation.

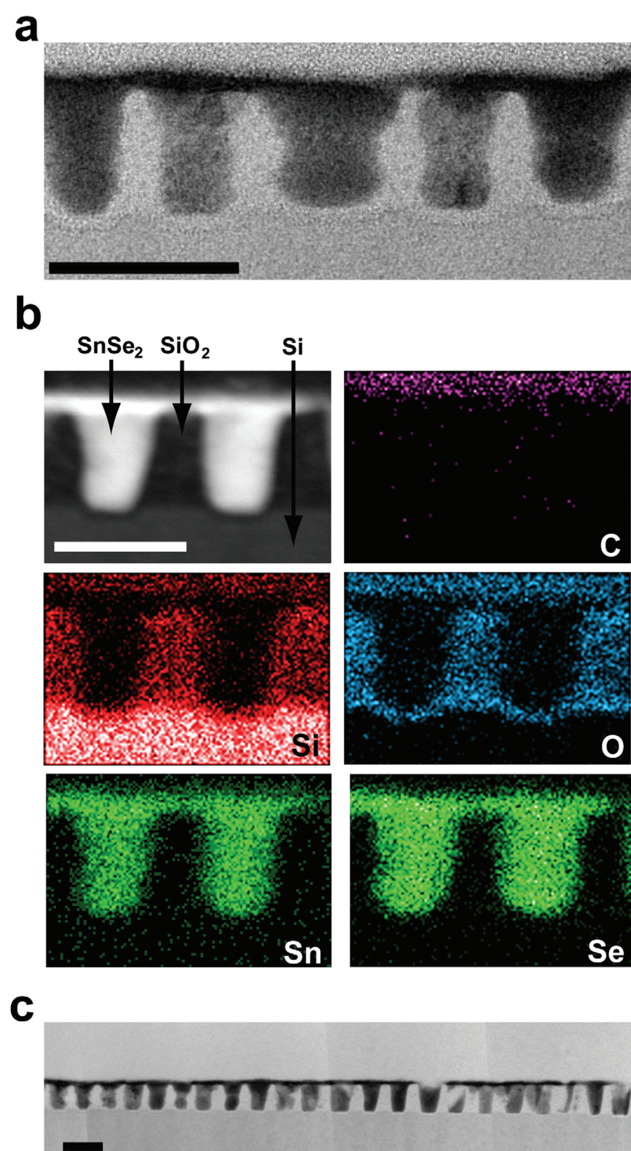

FIG. 6. (Color online) (a) Cross-sectional bright-field TEM image demonstrating high-quality $SnSe_2$ filling of the nanowells, (b) cross-sectional *z*-contrast TEM image along with corresponding EDS images showing the spatial locations of Sn, Se, Si, O, and C, and (c) cross-sectional bright-field TEM image with an expanded field of view. The scale bar is 50 nm in parts (a), (b), and (c).

IV. CONCLUSIONS

This work demonstrates a solution-phase deposition process for $SnSe_2$ phase change material and devices. The optical testing reveals very fast recrystallization times for $SnSe_2$. Our electrical testing also demonstrates that $SnSe_2$ can be switched electronically. Although the electronic devices performed poorly, this is likely due to their simple cell design as opposed to inherent $SnSe_2$ properties. Studies on $SnSe_2$ performance in conventional PCRAM cell architectures would reveal the full potential of $SnSe_2$ for PCRAM. Our demonstration of $SnSe_2$ deposition into nanowells also validates its potential for advanced PCRAM device architectures.

Future studies on phase change materials derived from solution-phase deposition of chalcogenidometallate clusters will also be interesting. For instance, the microstructure within the $SnSe_2$ films caused reflectivity variations, however varying the deposition and decomposition conditions may improve this. Additionally, the chalcogenidometallate cluster chemistry is applicable to a variety of material compositions, including the incorporation of dopants and/or the formation of alloys.[6,8,23] Chalcogenidometallate clusters have also been combined with colloidal nanoparticles to fabricate unique nanocomposite materials.[24] Nanoparticle composites exhibit a thermal conductivity reduction,[25] which is an effective means of reducing reset power.[1,26]

ACKNOWLEDGMENTS

We thank Professor Matthias Wuttig of RWTH Aachen University of Technology and Dr. Simone Raoux of IBM T.J. Watson Research Center for helpful discussions. We also thank Xiuhong Han from Nanolab Technologies for FIB preparation of the TEM sample and Brett Helms of the Molecular Foundry for providing PS-PMMA random copolymer. Work at the Molecular Foundry was supported by the Office of Science, Office of Basic Energy Sciences, of the U.S. Department of Energy under Contract No. DE-AC02-05CH11231. MAC is supported by the Stanford Non-Volatile Memory Technology Initiative. Work was performed in part at the Stanford Nanofabrication Facility (a member of the National Nanotechnology Infrastructure Network) which is supported by the National Science Foundation under Grant ECS-9731293, its lab members, and the industrial members of the Stanford Center for Integrated Systems.

[1]S. Raoux, W. Welnic, and D. Ielmini, Chem. Rev. **110**, 240 (2010).
[2]M. Wuttig and N. Yamada, Nat. Mater. **6**, 824 (2007).
[3]S.R. Ovshinsky, Phys. Rev. Lett. **21**, 1450 (1968).
[4]K. M. Chung, D. Wamwangi, M. Woda, M. Wuttig, and W. Bensch, J. Appl. Phys. **103**, 083523 (2008).
[5]M. Micoulaut, W. Welnic, and M. Wuttig, Phys. Rev. B **78**, 224209 (2008).
[6]D. J. Milliron, S. Raoux, R. Shelby, and J. Jordan-Sweet, Nat. Mater. **6**, 352 (2007).

[7]D. B. Mitzi, Inorg. Chem. **44**, 3755 (2005).
[8]D. B. Mitzi, Adv. Mater. **21**, 3141 (2009).
[9]D. B. Mitzi, L. L. Kosbar, C. E. Murray, M. Copel, and A. Afzali, Nature **428**, 299 (2004).
[10]D. B. Mitzi, S. Raoux, A. G. Schrott, M. Copel, A. Kellock, and J. Jordan-Sweet, Chem. Mater. **18**, 6278 (2006).
[11]Y. Chen, in *Phase Change Materials Science and Applications*, edited by S. Raoux and M. Wuttig (Springer, New York, 2009), pp. 331.
[12]D. J. Milliron, M. A. Caldwell, and H. S. P. Wong, Nano Lett. **7**, 3504 (2007).
[13]Nanolab Technologies, San Jose, CA, USA, *www.nanolabtechnologies.com*.
[14]See supplementary material at http://dx.doi.org/10.1063/1.3587187 for additional figures and experimental details.
[15]V. Weidenhof, I. Friedrich, S. Ziegler, and M. Wuttig, J. Appl. Phys. **86**, 5879 (1999).
[16]V. Weidenhof, I. Friedrich, S. Ziegler, and M. Wuttig, J. Appl. Phys. **89**, 3168 (2001).
[17]I. Friedrich, V. Weidenhof, W. Njoroge, P. Franz, and M. Wuttig, J. Appl. Phys. **87**, 4130 (2000).
[18]R. Bez, R.J. Gleixner, F. Pellizzer, A. Pirovano, and G. Atwood, in *Phase Change Materials Science and Applications*, edited by S. Raoux and M. Wuttig (Springer, New York, 2009), pp. 355.
[19]C. K. Chan, H. L. Peng, G. Liu, K. McIlwrath, X. F. Zhang, R. A. Huggins, and Y. Cui, Nat. Nanotechnol. **3**, 31 (2008).
[20]U. Russo, D. Ielmini, A. Redaelli, and A. L. Lacaita, IEEE Trans. Electron Devices **55**, 506 (2008).
[21]G. S. Sandhu, Thin Solid Films **320**, 1 (1998).
[22]D. J. Milliron, Q. Huang, and Y. Zhu, in *Phase Change Materials Science and Applications*, edited by S. Raoux and M. Wuttig (Springer, New York, 2009), pp. 227.
[23]R. Y. Wang, J. P. Feser, X. Gu, K. M. Yu, R. A. Segalman, A. Majumdar, D. J. Milliron, and J. J. Urban, Chem. Mater. **22**, 1943 (2010).
[24]R. Tangirala, J. L. Baker, A. P. Alivisatos, and D. J. Milliron, Angew. Chem., Int. Ed. **49**, 2878 (2010).
[25]W. Kim, R. Wang, and A. Majumdar, Nano Today **2**, 40 (2007).
[26]T. Y. Lee, K. H. P. Kim, D. S. Suh, C. Kim, Y. S. Kang, D. G. Cahill, D. Lee, M. H. Lee, M. H. Kwon, K. B. Kim, and Y. Khang, Appl. Phys. Lett. **94**, 243103 (2009).